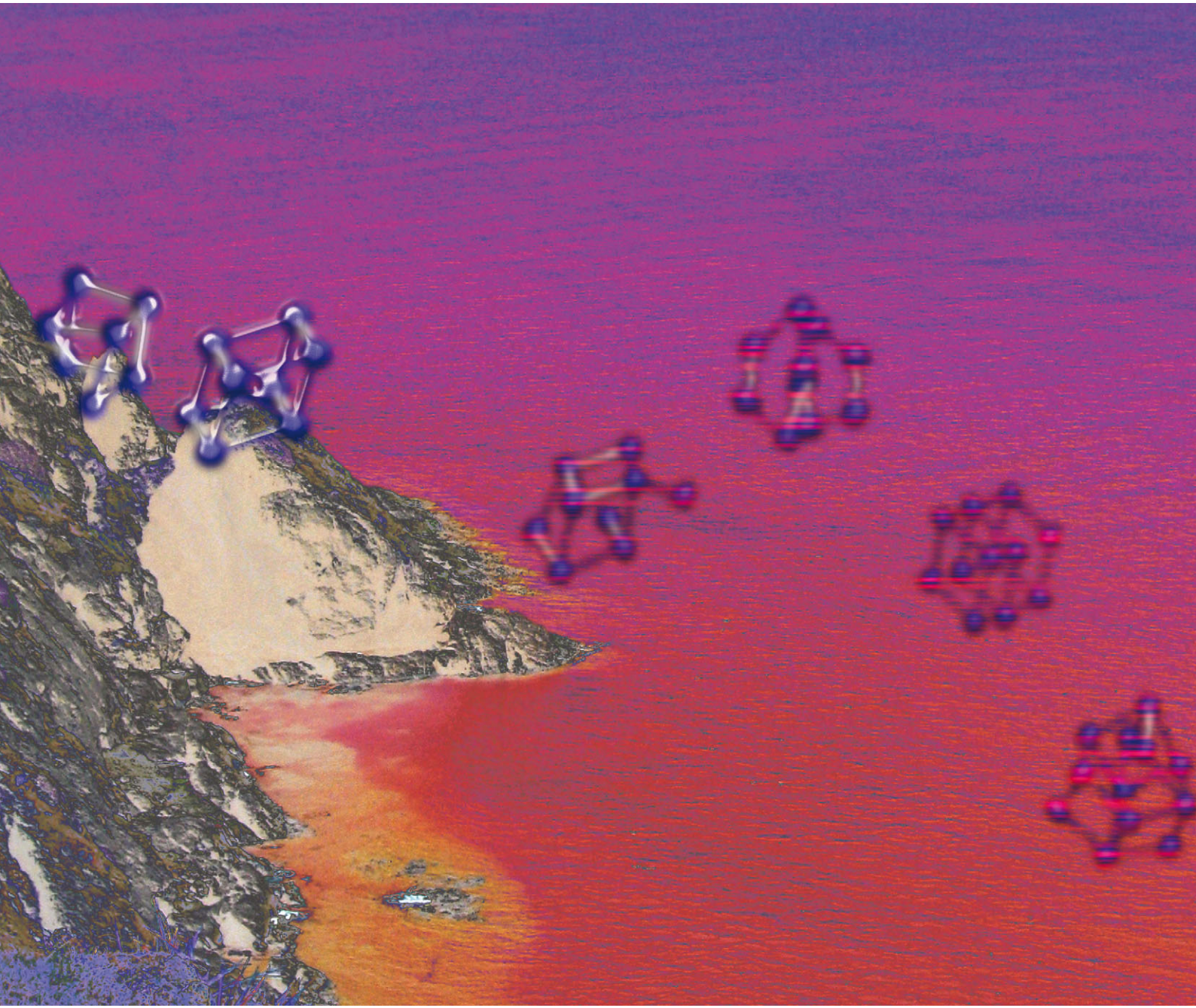


# PCCP

Physical Chemistry Chemical Physics

[www.rsc.org/pccp](http://www.rsc.org/pccp)

Volume 15 | Number 37 | 7 October 2013 | Pages 15245–15670



ISSN 1463-9076

**PAPER**

Steenbergen and Gaston

First-principles melting of gallium clusters down to nine atoms: structural and electronic contributions to melting



1463-9076(2013)15:37;1-I

# First-principles melting of gallium clusters down to nine atoms: structural and electronic contributions to melting

Cite this: *Phys. Chem. Chem. Phys.*, 2013, **15**, 15325

Krista G. Steenbergen and Nicola Gaston\*

First-principles Born–Oppenheimer molecular dynamics simulations of small gallium clusters, including parallel tempering, probe the distinction between cluster and molecule in the size range of 7–12 atoms. In contrast to the larger sizes, dynamic measures of structural change at finite temperature demonstrate that  $\text{Ga}_7$  and  $\text{Ga}_8$  do not melt, suggesting a size limit to melting in gallium exists at 9 atoms. Analysis of electronic structure further supports this size limit, additionally demonstrating that a covalent nature cannot be identified for clusters larger than the gallium dimer.  $\text{Ga}_9$ ,  $\text{Ga}_{10}$  and  $\text{Ga}_{11}$  melt at *greater-than-bulk* temperatures, with no evident covalent character. As  $\text{Ga}_{12}$  represents the first small gallium cluster to melt at a *lower-than-bulk* temperature, we examine the structural properties of each cluster at finite temperature in order to probe both the origins of greater-than-bulk melting, as well as the significant differences in melting temperatures induced by a single atom addition. Size-sensitive melting temperatures can be explained by both energetic and entropic differences between the solid and liquid phases for each cluster. We show that the lower-than-bulk melting temperature of the 12-atom cluster can be attributed to persistent pair bonding, reminiscent of the pairing observed in  $\alpha$ -gallium. This result supports the attribution of greater-than-bulk melting in gallium clusters to the anomalously low melting temperature of the bulk, due to its dimeric structure.

Received 19th April 2013,  
Accepted 5th June 2013

DOI: 10.1039/c3cp51690c

[www.rsc.org/pccp](http://www.rsc.org/pccp)

## 1 Introduction

Gallium is a fascinating element, both in its bulk form and at the nanoscale. It possesses one of the most diverse phase diagrams of the metallic elements, with non-standard pressure and temperature structures taking on modifications that include both boron-like molecular and close-packed metallic phases.<sup>1–5</sup> In the  $\alpha$ -phase of bulk gallium, known under standard conditions, there is one surprisingly short bond forming a covalently bound dimer at 2.44 Å. These dimers are arranged into buckled planes which have metallic character, leading to the description of gallium as a “molecular metal.”<sup>1,6</sup> Its various unique properties, such as anisotropic conductivity<sup>7</sup> and an anomalously low melting temperature, have long been attributed to this coexistence of covalent and metallic bonding; however, evidence of the effect of the dimeric structure on melting remains inconclusive.<sup>8,9</sup>

Small clusters of gallium are useful model systems for understanding bonding in the bulk, as they have demonstrated

structures closely related to the  $\alpha$ -phase with bond lengths mimicking the first and second nearest neighbor distances of 2.44 and 2.71 Å.<sup>10,11</sup> As melting temperature measurements of small gallium clusters<sup>12</sup> have revealed melting temperatures starkly contrasting the low melting point of bulk, finite temperature characteristics of these clusters can be usefully contrasted with bulk thermodynamic properties. In contrast to the usual melting point depression observed for small particles, gallium clusters in the size range of 17–55 atoms remain solid at twice the bulk melting temperature.<sup>13,14</sup> Moreover, the addition of a single atom can change the melting temperature by as much as 80 K. These observations highlight the need to better understand the nature of melting in these small cluster sizes.

A series of computational studies addressing small gallium cluster melting concluded that greater-than-bulk melting in gallium clusters could be attributed to a different kind of covalent bonding in the clusters than is found in bulk.<sup>15–17</sup> More recent work, however, has questioned the earlier claim of covalency in small gallium clusters.<sup>18,19</sup> While evidence of a metallic character has been reported by these studies,<sup>18,19</sup> a conclusive means of determining the relationship between structural motifs and electronic structure has yet to be firmly established.<sup>20</sup> This is an intriguing and important task, given

MacDiarmid Institute for Advanced Materials and Nanotechnology,  
Victoria University of Wellington, P.O. Box 600, Wellington 6012, New Zealand.  
E-mail: [nicola.gaston@vuw.ac.nz](mailto:nicola.gaston@vuw.ac.nz)

the great structural diversity of experimentally characterized gallium clusters even among the smallest cluster sizes.<sup>1</sup>

At the smallest sizes, however, experimental melting is hindered by low internal energy of the structures. As phase transitions are identified by a peak in the specific heat curve due to the release of latent heat, which decreases with size,<sup>21</sup> phase transitions for very small clusters become less well-defined.<sup>13,22</sup> Experimental specific heat measurements for the smallest unsupported sizes include  $\text{Ga}_{17}^+$  and  $\text{Al}_{16}^+$ , which exhibit rather featureless specific heat curves without clearly defined melting transitions.<sup>13,23</sup>

The fact that experimental reports are lacking for  $n < 16$ , where  $n$  is the number of atoms, has not prevented theoretical investigations. Research investigating the global minimum (GM) for 2–12 atom clusters of sodium,<sup>24</sup> tin,<sup>25</sup> gallium,<sup>10,11,26</sup> and aluminum<sup>27</sup> have revealed an intriguing odd-even motif in several properties, such as cohesive energy second order differences and average coordination number. Molecular dynamics (MD) melting simulations have been completed for 2–12 atom clusters of sodium,<sup>28–31</sup> argon,<sup>32–35</sup> gold,<sup>36</sup> silver,<sup>37</sup> lithium,<sup>38</sup> tin,<sup>39</sup> and aluminum.<sup>40</sup> However, aside from classical MD simulations of small aluminum clusters<sup>40</sup> and first-principles studies of larger sodium clusters,<sup>41,42</sup> each of these studies investigates individual sizes, without addressing how melting changes across the size range. To our knowledge, first-principles melting simulations for these very small cluster sizes have never systematically addressed thermodynamic changes over an extended size-range.

Taking a methodical approach to the effect of size, we present the results of density functional theory (DFT) based Born–Oppenheimer molecular dynamics simulations for gallium clusters between 7–12 atoms. We implement a parallel tempering molecular dynamics (PTMD) algorithm<sup>43</sup> to fully explore the complex potential energy surfaces occupied by these clusters, thereby extending previous research on the global minimum (GM) structures for small gallium clusters<sup>10</sup> and greater-than-bulk melting behavior of gallium.<sup>19</sup>

We compute specific heat curves for each cluster, systematically investigating thermodynamic changes induced by single-atom additions across the size range. Including electronic structure, thermodynamic and finite temperature structural analyses, we establish a lower size-limit to melting in gallium. Below this size-limit, we observe thermodynamic behavior more characteristic of molecules than clusters, with finite temperature behavior dominated by vibrational motion. We probe the contributions to size-sensitive melting temperatures through an analysis of energetic and entropic differences between the solid and liquid phases. Finally, we complete a finite temperature analysis of pair bonding in order to answer the more general question of how bonding affects the melting behavior of these small clusters, providing important insights into the mechanisms underlying both the greater-than-bulk melting phenomenon as well as the low melting temperature observed in bulk gallium.

## 2 Computational methods

All calculations utilized Vienna Ab Initio Software Package (VASP) 5.2,<sup>44–47</sup> with GGA-PW91 functional<sup>48,49</sup> coupled with

projector-augmented wave (PAW) pseudopotentials.<sup>50,51</sup> As our previous research revealed negligible thermodynamic differences between the valence and core d-electron models,<sup>19</sup> we treat only the  $3s^23p^1$  as valence electrons. Geometry optimizations used an energy cut-off of 350 eV, while molecular dynamics (MD) calculations used 134.7 eV (default value for the pseudopotential). For both optimizations and MD, we added full dipole corrections in all directions to account for VASP's treatment of charge under periodic boundary conditions.

The optimization for  $\text{Ga}_{12}$  was initialized with a symmetric icosahedron, while  $\text{Ga}_7$  and  $\text{Ga}_8$  were initialized with rhomboid structures. The remainder of the cluster optimizations were seeded with stacked pentagonal/hexagonal plane-themed structures. The initial structures are illustrated in Fig. 1, along with their cohesive energies calculated as  $E_{\text{coh}} = E_{\text{1Ga}} - E/n$ .

Each initial structure provides only a low-energy starting point for the molecular dynamics simulations. The PTMD algorithm,<sup>43</sup> which allows for swapping between configurations at different energies, is implemented in order to ensure adequate exploration of configuration space and sampling of the GM structure. The optimized structures were used to initialize short (10 ps) canonical molecular dynamics equilibration runs. Set at 19 different temperatures per cluster, we utilize only the configuration and velocities from the final canonical time step to seed subsequent microcanonical molecular dynamics simulations. The combination of canonical–microcanonical equilibration yielded a set of 19 (approx.) evenly spaced constant energy simulations per cluster, ensuring our calculations covered the experimental temperature range of interest. The canonical equilibrations were not included in any subsequent analysis.

PTMD simulations for each cluster sized 7–12 atoms were run for 190, 360, 220, 220, 280 and 210 ps, respectively. The lowest energy structures obtained in each parallel tempering

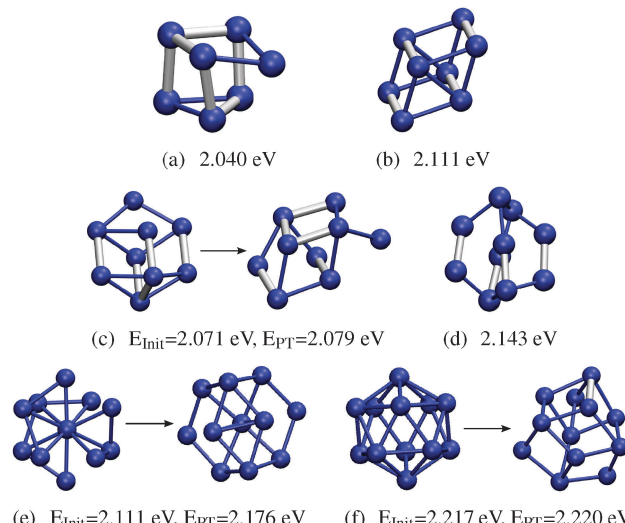


**Fig. 1** Initial and PT-derived structures for each cluster size, as well as the cohesive energies. Where the PT-derived structure varied notably from the initial geometry, the initial structure is given to the left of the arrow with the PT structure to the right. Bond length differences are illustrated as:  $r_{12} < 2.6 \text{ \AA}$  in thicker-radius silver, while  $2.6 \text{ \AA} < r_{12} < 2.8 \text{ \AA}$  are blue.

simulation (PT-derived) are compared to the initial structure, as illustrated in Fig. 1. The PT-derived structures for the 7, 8 and 10-atom clusters were identical to their initial configurations, while PTMD identifies different structures with notably higher cohesive energies for Ga<sub>9</sub>, Ga<sub>11</sub> and Ga<sub>12</sub>.

The putative GM for Ga<sub>8</sub> is a highly symmetric rhomboid reminiscent of bulk gallium, with the shortest bonds at  $\sim 2.49 \text{ \AA}$  and the next nearest neighbors at  $2.71 \text{ \AA}$ .<sup>10</sup> The PT-derived structure for Ga<sub>7</sub> and Ga<sub>9</sub> respectively add or subtract a single atom to the Ga<sub>8</sub> rhomboid, distorting its symmetry. Both Ga<sub>10</sub> and Ga<sub>11</sub> are symmetric clusters. For Ga<sub>11</sub>, the PT-derived structure has a butterfly motif containing two Ga<sub>8</sub> rhomboids sharing 5 central atoms. A distorted rhomboid can also be identified in the 12-atom structure.

### 3 Results

#### 3.1 Solid-liquid phase transition

Multiple histogram (MH) analysis<sup>28,52–54</sup> yielded the set of canonical specific heat curves illustrated in Fig. 2. Only Ga<sub>10</sub>, Ga<sub>11</sub> and Ga<sub>12</sub> demonstrate well-defined peaks that can be clearly attributed to a melting phase transition. In order to further explore the question of how these small clusters melt, we analyzed the root-mean square bond length deviation ( $\delta_{\text{rms}}$ ). Measuring bond length variance, this quantity is calculated as

$$\delta_{\text{rms}} = \frac{2}{n(n-1)} \sum_{i>j} \frac{(\langle r_{ij}^2 \rangle_t - \langle r_{ij} \rangle_t^2)^{1/2}}{\langle r_{ij} \rangle_t}, \quad (1)$$

where  $n$  is the total number of atoms,  $r_{ij}$  represents the bond length between atoms  $i$  and  $j$  within the cluster at time  $t$ , and  $\langle \cdot \rangle_t$  represents the time average of the quantity within the brackets. This analysis yields an indication of structure rigidity at a given temperature, with a sharp increase in  $\delta_{\text{rms}}$  signaling a melting transition. Due to parallel tempering configuration swapping, exact values of  $\delta_{\text{rms}}$  should be taken with caution in the region  $\sim 100 \text{ K}$  to each side of the melting temperature. However, careful testing showed that the overall nature of the changes in  $\delta_{\text{rms}}$ , from a characteristic ‘solid-like’ to a ‘liquid-like’

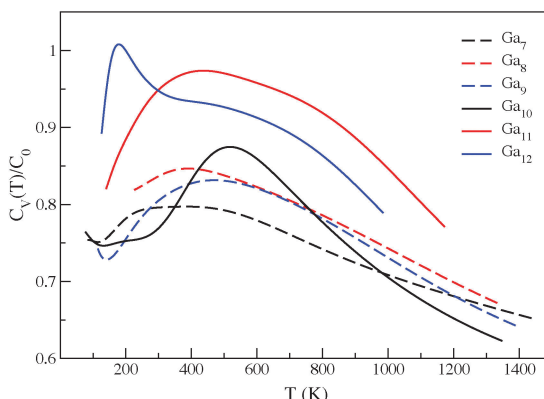


**Fig. 2** Canonical specific heat curves for the 7–12 atom clusters, normalized to the classical specific heat accounting for rotational and vibrational degrees of freedom,  $C_0 = (3n - 6 + 3/2)k_B$ .

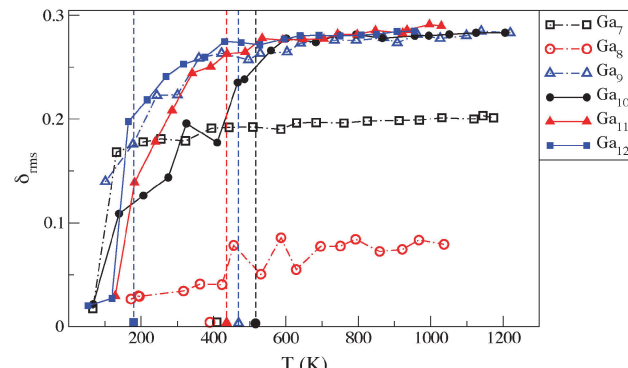


**Fig. 3** For each small cluster,  $\delta_{\text{rms}}$  is plotted against the average temperature. The location of  $T_{\text{peak}}$  for the four largest clusters (from Fig. 2) are annotated by vertical dashed lines and corresponding symbols on the x-axis, while the 7 and 8-atom  $T_{\text{peak}}$  is annotated only by symbols along the x-axis.

value, were minimally affected in our simulations by parallel tempering.

The use of parallel tempering as well as the small cluster sizes make the increase in  $\delta_{\text{rms}}$  more gradual and inexact as a measure of melting temperature, as has been demonstrated in previous work.<sup>31</sup> However, the rise in  $\delta_{\text{rms}}$  correlates nonetheless with the peak temperatures extracted from the specific heat curves, as illustrated in Fig. 3. The 10, 11 and 12-atom clusters exhibit a well-defined  $\delta_{\text{rms}}$  melting signature, with low-temperature deviations at just above zero followed by a steep rise to  $\sim 0.28$ .

Although the lowest temperature value of  $\delta_{\text{rms}}$  for Ga<sub>9</sub> is relatively high at  $\sim 0.14$ , this arises from destabilization of the 8-atom rhomboid resulting in significantly increased mobilities for two atoms sharing the rhomboid ad-atom position of the PT-derived structure (illustrated in Fig. 1(c)). This high initial value for the 9-atom cluster is followed by a rise and similar convergence to  $\delta_{\text{rms}} = 0.28$  at higher temperatures. For the 9–12 atom clusters, the temperature corresponding to the maximum specific heat is annotated by the vertical dashed line and corresponding symbol along the x-axis in Fig. 3. Above these  $T_{\text{peak}}$  values,  $\delta_{\text{rms}}$  converges to a smooth progression with increasing temperature, characteristic of the liquid state for these clusters. This is corroborated by inspection of the time-average pair distribution function given in Fig. 4, where we see convergence in the structure function at high temperatures for Ga<sub>9</sub>–Ga<sub>12</sub>, but not for the smaller clusters.

The root mean square deviations remain low across the range of temperatures for both the 7 and 8-atom clusters, indicating highly rigid structures persist even at high temperatures. The 8-atom  $\delta_{\text{rms}}$  curve shows no signs of melting.<sup>†</sup> While Ga<sub>7</sub> exhibits a similar  $\delta_{\text{rms}}$  signature to those of the larger clusters, it converges to a value of only  $\sim 0.2$ . Additionally, a comparison of the  $T_{\text{peak}}$  from Fig. 2 (marked by corresponding

<sup>†</sup> In order to verify that melting did not occur at a higher temperature for the 8-atom cluster, we completed additional simulations up to an average temperature of 2440 K. No specific heat peak is noted and the  $\delta_{\text{rms}}$  behavior remains unique in this higher temperature range.

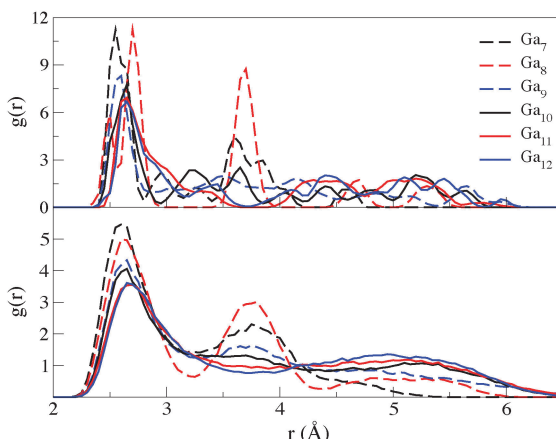


**Fig. 4** Time-average pair distribution function for each cluster (top) at the lowest temperature, where each cluster exhibits a unique structural signature, and (bottom) at the highest temperature, where clusters sized 9–12 demonstrate a similar liquid structure while the 7- and 8-atom signatures remain unique.

symbols on the  $x$ -axis) with the  $\delta_{\text{rms}}$  behavior provides no support for the interpretation of these peaks as due to a melting transition.

An analysis of the atomic mean square displacements (MSD)<sup>19</sup> offers additional insight. The MSD for atom  $i$  is defined as

$$\langle r_i^2(t) \rangle = \frac{1}{M} \sum_{m=1}^M [R_i(t_{0m} + t) - R_i(t_{0m})]^2 \quad (2)$$

where  $t$  is the time over which the atomic displacement is measured,  $t_{0m}$  is a selected time origin and  $M$  is the total number of time origins sampled.  $R_i(t_{0m})$  specifies the coordinates of the  $i$ th atom at the  $m$ th time origin and  $R_i(t_{0m} + t)$  represents the coordinates of the  $i$ th atom after time  $t$  has passed since the  $m$ th time origin. In taking reference structures from multiple time origins against which to measure displacement, MSD avoids the complication of choosing a single reference structure from the hundreds of thousands of structures explored in the course of an MD simulation.

Calculated between parallel tempering swaps, this measure tracks the mobility of individual atoms and yields a picture of how clusters melt when the effect of parallel tempering is excluded. For these small gallium clusters, a very clear difference can be observed between the mobility of interior and surface atoms.<sup>19</sup> The MSD for  $\text{Ga}_8$  contrasts starkly with expected behavior, exhibiting coupled atomic motion for all temperatures. Due to symmetry, each visible line in Fig. 5 displays the overlapping trace of two different atoms, illustrating the strong pair bonding that remains in this cluster even at the highest temperature.

This is in contrast with the atomic mobilities for the 9–12 atom clusters, exemplified in Fig. 5 by the low-temperature MSD for  $\text{Ga}_{12}$ . At low simulation temperatures, these clusters exhibit low atomic mobilities for highly coordinated atoms and high mobilities for atoms with lower coordination numbers; however, all atoms become equally mobile at temperatures above  $T_{\text{peak}}$ . For the 10–12 atom clusters, the highly coordinated

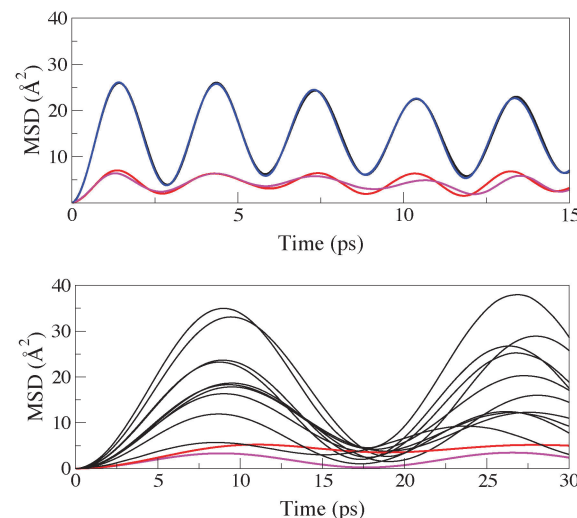


**Fig. 5** (top) MSD for  $\text{Ga}_8$  at the highest temperature, representative of the MSD at all temperatures for the 8-atom cluster. Atomic motion is coupled in the 8-atom cluster, such that each line represents 2 atoms. (bottom) MSD for  $\text{Ga}_{12}$  at the lowest temperature, illustrating the lower mobility for the highly-coordinated atoms, represented in red and magenta (grey) compared to the atoms with lower atomic coordination (black). These atoms become equally mobile at temperatures above melting.

atoms with low atomic mobility are the central atoms, which can be identified by their red or pink shading in Fig. 6. As neither  $\text{Ga}_7$  nor  $\text{Ga}_8$  exhibits characteristic melting behavior in the specific heat,  $\delta_{\text{rms}}$  or MSD analyses, we consider this to demonstrate a lower size-limit to melting in gallium clusters at 9-atoms. Below 9 atoms, we observe thermodynamic behavior more characteristic of molecules than clusters.

### 3.2 Electronic structure

**3.2.1 Bader analysis illustrates charge polarization.** This size limit is further evidenced by an analysis of partial charge for each of the PT-derived lowest energy structures. Bader analysis of partial charge<sup>55</sup> uses electron density minima to assign charge volumes around each ion. The total charge contained within that volume is integrated, yielding a partial charge assigned to each ion in the structure. As illustrated in Fig. 6, Bader analysis produces neutral atomic charges for  $\text{Ga}_7$  and  $\text{Ga}_8$ . At all larger sizes, partial charges were noted for particular atoms. The protruding atom in the 9-atom cluster was slightly positively charged while  $\text{Ga}_{10}$  has two, negatively charged central atoms. The 11 and 12-atom clusters demonstrate charge polarization, with negatively charged central atoms and positive protruding atoms. This polarization marks the beginning of a distinction between interior and surface atoms, necessary to the definition of a cluster as a finite piece of a bulk material.

**3.2.2 ELF analysis illustrates the lack of covalency.** A second measure of electronic structure, electron localization function (ELF) analysis,<sup>56–58</sup> measures the probability of finding a second electron spatially localized with a reference electron. ELF analysis can be a useful tool in visualizing the nature of bonding, to

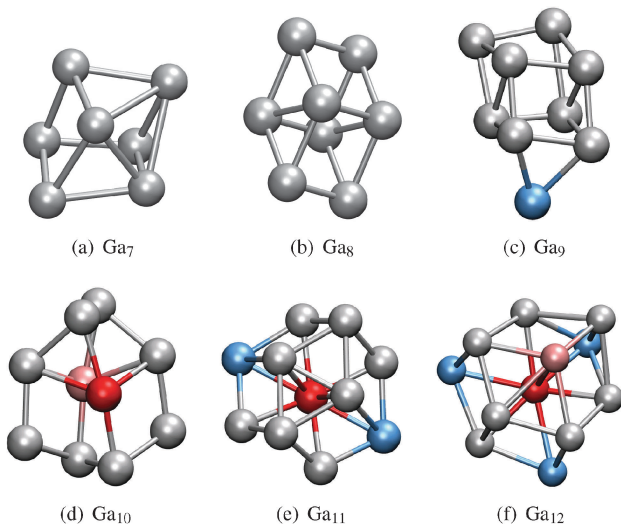


**Fig. 6** Bader analysis of partial charge,  $q_p$ , for each small cluster: (red)  $q_p < -0.2e$ ; (pink)  $-0.2e < q_p < -0.1e$ ; (silver)  $-0.1e < q_p < 0.1e$ ; and (light blue)  $0.1e < q_p < 0.2e$ .

include metallic or covalent character. Previous studies of small gallium clusters have used ELF to characterize the nature of bonding in the clusters,<sup>15–17</sup> attributing the greater-than-bulk melting to ELF-identified covalent bonding that differed in nature from bulk covalency.

ELF covalency can be visually identified by a region of high electron localization centered on the bond between two atoms. As illustrated in Fig. 7, ELF analysis of both the gallium dimer and bulk  $\alpha$ -gallium clearly identifies covalency for each system. However, contrasting starkly with the dimer and bulk, ELF analyses for the gallium trimer and tetramer demonstrate only

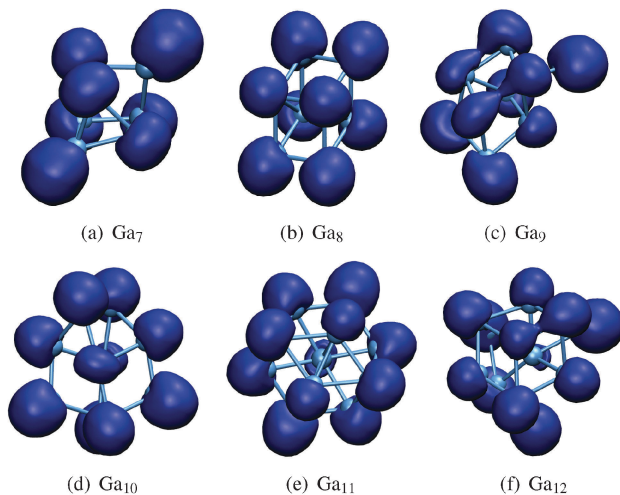


**Fig. 8** ELF analysis, at ELF = 0.65 isovalue, for the PT-derived lowest energy structures of each small cluster sized 7–12 atoms. All clusters demonstrate ion-centered electron localization with no evidence of covalency. It should be noted that in the 9 and 12-atom clusters, the region of electron localization seeming to link two atoms does *not* represent covalency, but are simply regions of ion-centered electron localization overlapping due to a shorter bond length.

ion-centered ELF, with no evidence of covalency.<sup>‡</sup> In fact, aside from the gallium dimer, all 16 cluster sizes we have analyzed to date<sup>§</sup> reveal ion-centered, non-covalent electron localization.

Fig. 8 illustrates the ELF results for each cluster sized 7–12 atoms, again demonstrating ion-centered electron localization with no evidence of covalency. This applies even to the 8-atom cluster despite apparent pair bonding similar to that of bulk gallium. As previous studies of small gallium clusters show the same ion-centered electron localization,<sup>15–17</sup> we are unable to support the attribution of covalent character to bonding in small gallium clusters based on ELF analysis.

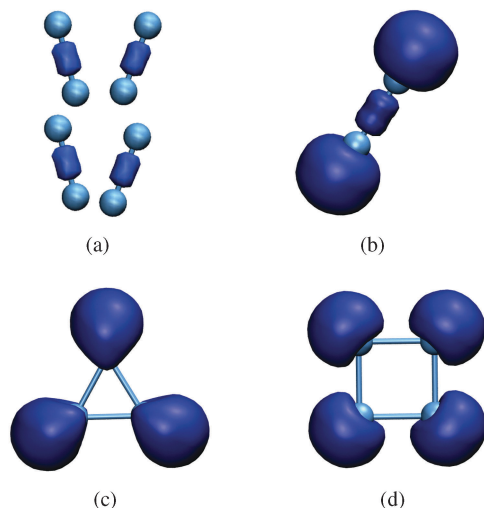


**Fig. 7** ELF analysis, at ELF = 0.65 isovalue, illustrating covalency for the (a)  $\alpha$ -gallium bulk unit cell<sup>20</sup> and (b) gallium dimer. The region of electron localization centered on each bond between two atoms identifies the covalent bonds. This is contrasted with the ELF analysis for the (c) trimer and (d) tetramer, demonstrating ion-centered electron localization with no evidence of covalency. Although not presented here, these ELF results are also representative of the 5 and 6-atom gallium molecules.

## 4 Discussion

The lack of covalency, as indicated by ELF analysis, requires us to look for a different explanation of the greater-than-bulk melting observed in these small gallium clusters. Greater-than-bulk melting temperatures were observed for the 9–11 atom clusters at 469 K, 517 K and 436 K respectively (bulk  $\alpha$ -gallium melts at 303 K). However, the 12-atom cluster exhibits a melting transition at 178 K. At  $\sim$ 300 K below any experimentally measured or theoretically simulated cluster melting temperature, Ga<sub>12</sub> is the first small gallium cluster to exhibit a lower-than-bulk melting temperature. This result affords us the opportunity to explore the underlying mechanism of both greater-than-bulk melting, as well as the large variation in melting temperature observed with just one-atom additions to the structures.

<sup>‡</sup> Initial geometries for the 2–6 atom clusters were obtained from our previous work.<sup>10</sup> These configurations were then optimized for the GGA-PW91 functional according to the methods listed above. The ELF analysis for the bulk unit cell are repeated from our previous research.<sup>20</sup>

<sup>§</sup> We have completed the ELF analysis for optimized structures of 2–12, 20 and 32–36 atom gallium clusters.

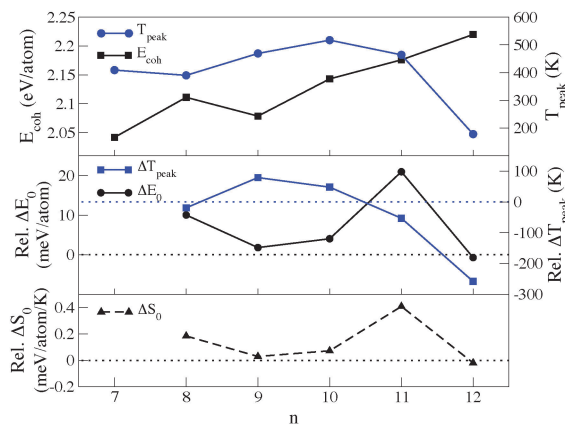


**Fig. 9** (top)  $E_{\text{coh}}$  for each PT-derived structure and the temperature of the specific heat curve peak,  $T_{\text{peak}}$ , illustrating the lack of correlation. (middle and bottom) The relative (Rel.) energy and entropy offsets contributing to differences in  $T_{\text{peak}}$  between cluster sizes, where  $\Delta X = X_n - X_{(n-1)}$ ,  $X = \{T_{\text{peak}}, E_0, S_0\}$ . A positive Rel.  $\Delta E_0$  and negative Rel.  $\Delta S_0$  contribute to a higher melting temperature for the  $n$ -atom cluster compared to the  $(n-1)$ -atom cluster. A positive  $\Delta T_{\text{peak}}$  indicates a higher  $T_{\text{peak}}$  for the  $n$ -atom cluster.

Starting with the cohesive energy trends for each cluster size, a comparison of  $E_{\text{coh}}$  to the specific heat peak temperature demonstrates no correlation, as illustrated in the top panel of Fig. 9. An alternative to looking at individual  $T_{\text{peak}}$  values is to look at the  $\Delta T_{\text{peak}}$  associated with the addition of a single atom. These changes in melting temperature can then be compared to the energetic and entropic differences between the solid and liquid phases of each cluster. In accordance with the methods presented by Schmidt *et al.*,<sup>59</sup> the energy offset ( $\Delta E_0$ ) is computed by comparing the solid and liquid branches of the multiple histogram (MH) caloric curves between two cluster sizes. The entropy offset ( $\Delta S_0$ ) is then obtained by a fit to the solid and liquid branches of the MH entropy curve. We calculate the  $\Delta E_0$  and  $\Delta S_0$  for each cluster size  $n$  relative to cluster size  $(n-1)$ .

Fig. 9 (middle and bottom panels) illustrates both the energetic and entropic contributions to the changes in the observed peak temperatures. As the 7 and 8-atom clusters do not appear to melt according to our previous analyses, comparisons for these sizes are provided only for completeness. The relative energetic differences between solid and liquid phases correlate well with melting temperature differences for the 9 and 10-atom clusters. For the 11-atom cluster, however, entropic effects are clearly dominant. For  $\text{Ga}_{11}$ ,  $T_{\text{peak}}$  is lower than that of the  $(n-1)$  cluster size, in contrast with the large positive  $\Delta E_0$  for this cluster. Instead, this energetic influence is countered by the large positive  $\Delta S_0$  value, which serves to lower  $T_{\text{peak}}$ . This strong entropic influence for  $n=11$  arises from the highly symmetric nature of its lowest energy (PT-derived) structure. As the  $\Delta E_0$  and  $\Delta S_0$  values are nearly zero for the 12-atom cluster, its lower-than-bulk melting temperature does not correlate with either energetic or entropic trends.

Further exploring the low melting temperature for  $\text{Ga}_{12}$ , we completed an analysis of pair bonding at finite temperature in order to probe structural or bonding similarities to bulk gallium.

For each time step between parallel tempering configuration swaps, we measure the interatomic pair separations ( $r_{ij}$ ) for all atoms within the cluster. Tracking the percentage of total simulation time that two atoms remain pair bonded, defined as  $r_{ij} < 2.5 \text{ \AA}$ , we calculate the pair persistence at each average temperature according to

$$\text{PP}_{ij} = \frac{\sum_{t=1}^T X_{ij}(t)}{T} \quad (3)$$

where  $T$  is the total time and  $X_{ij}(t)$ , representing the atomic separation between atom  $i$  and atom  $j$  at time step  $t$ , is given as

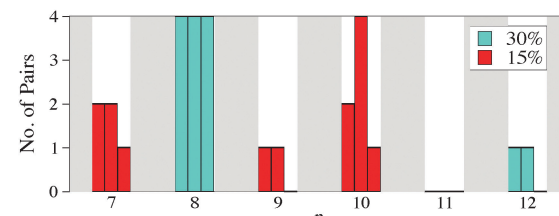
$$X_{ij}(t) = \begin{cases} 1 & \text{if } r_{ij} \leq 2.5 \text{ \AA} \\ 0 & \text{if } r_{ij} > 2.5 \text{ \AA} \end{cases}. \quad (4)$$

Fig. 10 illustrates the number of pair bonds that persist more than 30% and 15% of the simulation time at 3 different finite temperatures: the lowest temperature, a temperature just above the melting transition and at one of the highest average temperatures all simulations reach ( $\sim 1000$  K).

Pair bonding within the 8-atom cluster remains significant across the range of temperatures, as was also noted in the MSD analysis. However, of the clusters that exhibit a melting transition ( $n \geq 9$  atoms),  $\text{Ga}_{12}$  is the only cluster that exhibits strongly persistent pair bonding, as indicated by the 30% persistence measure. This strong bond remains even within the liquid structure at a temperature just above melting.

The unique nature of pairing in the 12-atom cluster is further evidenced in Fig. 11, illustrating the maximum pair persistence (MPP) and 2nd maximum pair persistence (2MPP) for each melting cluster size ( $n \geq 9$  atoms). For the 9–11 atom clusters, the MPP remains below 30% across the range of temperatures. Additionally, there is minimal difference between MPP and 2MPP for the 9–11 atom clusters, remaining between 0–15% at all temperatures. For  $\text{Ga}_{12}$ , however, the MPP at the lowest temperature is remarkably high ( $\sim 45\%$ ) and there is a significant difference between the MPP and 2MPP. This pair remains more persistently bound than the 9–11 atom clusters up to 110 K beyond the melting temperature for  $\text{Ga}_{12}$ .

This is an extraordinary feature, noting that  $\text{Ga}_9$ ,  $\text{Ga}_{10}$  and  $\text{Ga}_{11}$  are solid at this temperature, and leads to the question of



**Fig. 10** Bar plot illustrating the number of covalent-like pair bonds ( $r < 2.5 \text{ \AA}$ ) that persist at least 15% or 30% of the simulation time at (left bar) the lowest temperature, (middle bar) the temperature just above the peak specific heat temperature (low temperature liquid for the 9–12 atom clusters) and (right bar) the temperature corresponding to  $\sim 1000$  K average temperature. The unfilled bars demonstrate the absence of pairs persisting more than 15% of the time.

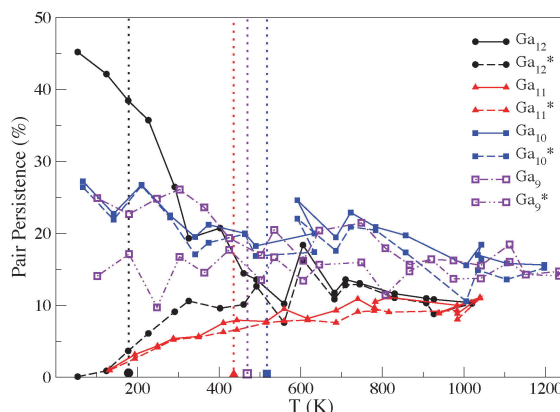


**Fig. 11** The maximum pair persistence (designated  $\text{Ga}_n$ ) and 2nd maximum pair persistence (designated  $\text{Ga}_n^*$ ) for each of the melting cluster sizes ( $n \geq 9$ ), with melting temperatures indicated by the dotted vertical line and corresponding symbol along the x-axis. The difference between the MPP and 2MPP, as indicated by the separation between lines of the same color, is minimal for the 9–11 atom clusters at all temperatures. This difference is significant for  $\text{Ga}_{12}$ , even at temperatures 110 K above the melting transition.

why  $\text{Ga}_{12}$  is unique in this respect. Electronically, none of the clusters in the size-range considered here have ‘magic number’ shell closings, with 21, 24, 27, 30, 33, and 36 electrons. However, if the strong pairing in the 12-atom cluster represents the formation of a single covalent bond, this would reduce the number of delocalized electrons to 34, which corresponds to the complete filling of the 1F shell in the spherical jellium model.<sup>60</sup> This presents a possible rationale for the unique thermodynamic behavior of  $\text{Ga}_{12}$  that is most reminiscent of bulk gallium,<sup>9</sup> which likely factors into the lower-than-bulk melting temperature for this cluster size. This result also supports the attribution of the anomalously low melting temperature in bulk  $\alpha$ -gallium to its dimeric structure.

## 5 Conclusions

In summary, the combination of MH specific heat and  $\delta_{\text{rms}}$  analyses can distinguish melting transitions for gallium clusters with as few as 9-atoms. We report a solid–liquid phase transition for  $\text{Ga}_9$ ,  $\text{Ga}_{10}$ ,  $\text{Ga}_{11}$  and  $\text{Ga}_{12}$  at 469 K, 517 K, 436 K and 178 K, respectively. The melting temperatures for the 9, 10 and 11-atom clusters follow the greater-than-bulk melting temperature trend experimentally observed for larger clusters.<sup>13,14</sup>

However, in the first demonstration that the greater-than-bulk melting trend does not universally apply to all small gallium clusters, the melting temperature for  $\text{Ga}_{12}$  is significantly lower than that of bulk gallium. This lower-than-bulk melting temperature stems from a strong pair bond that persists even above the cluster melting temperature, exhibiting a marked similarity to bulk thermodynamic behavior.<sup>9</sup> We theorize that this strongly persistent pair represents a covalent bond at finite temperature which reduces the number of delocalized valence electrons to 34, thus creating a closed electron shell in the simple jellium model.<sup>60</sup> Unfortunately, covalency at finite temperature cannot be resolved with currently

available methods of electronic structure analysis, highlighting a need for future development.

The 7 and 8-atom clusters reveal no signs of melting. Their unique  $\delta_{\text{rms}}$  curves coupled with the distinct high-temperature MSD profiles indicate that these clusters fall outside of the realm of “normal” cluster thermodynamics, setting a lower bound to the cluster size at which melting is observed. We propose this thermodynamic limit may be best understood as a cluster-to-molecule transition for these small systems.

## Acknowledgements

This work was supported by the Royal Society of New Zealand Marsden Fund contract number IRL0801. We also thank the New Zealand eScience Infrastructure (NeSI), particularly the BlueFern (University of Canterbury, nesi67) and Pan (University of Auckland, nesi7) supercomputer teams for computational time and excellent support.

## References

- 1 A. Schnepf and H. Schnöckel, *Angew. Chem., Int. Ed.*, 2002, **41**, 3532–3554.
- 2 (a) L. Bosio, H. Curien, M. Dupont and A. Rimsky, *Acta Crystallogr., Sect. B: Struct. Crystallogr. Cryst. Chem.*, 1973, **29**, 367–368; (b) L. Bosio, A. Defrain, H. Curien and A. Rimsky, *Acta Crystallogr., Sect. B: Struct. Crystallogr. Cryst. Chem.*, 1969, **25**, 995; (c) L. Bosio, H. Curien, M. Dupont and A. Rimsky, *Acta Crystallogr., Sect. B: Struct. Crystallogr. Cryst. Chem.*, 1972, **28**, 1974–1975.
- 3 L. Bosio, *J. Chem. Phys.*, 1978, **68**, 1221.
- 4 O. Schulte and W. Holzapfel, *Phys. Rev. B: Condens. Matter Mater. Phys.*, 1997, **55**, 8122.
- 5 T. Kenichi, K. Kazuaki and A. Masao, *Phys. Rev. B: Condens. Matter Mater. Phys.*, 1998, **58**, 2482.
- 6 X. Gong, G. Chiarotti, M. Parrinello and E. Tosatti, *Phys. Rev. B: Condens. Matter Mater. Phys.*, 1991, **43**, 14277–14280.
- 7 R. Powell, *Proc. R. Soc. London, Ser. A*, 1951, **209**, 525–541.
- 8 X. Gong, G. Chiarotti, M. Parrinello and E. Tosatti, *Europhys. Lett.*, 1993, **21**, 469.
- 9 K. Tsai, T. Wu and S. Tsay, *J. Chem. Phys.*, 2010, **132**, 034502.
- 10 N. Gaston and A. Parker, *Chem. Phys. Lett.*, 2011, **501**, 375–378.
- 11 N. Drebov, F. Weigend and R. Ahlrichs, *J. Chem. Phys.*, 2011, **135**, 044314.
- 12 C. Neal, A. Starace and M. Jarrold, *J. Am. Soc. Mass Spectrom.*, 2007, **18**, 74–81.
- 13 G. Breaux, R. Benirschke, T. Sugai, B. Kinnear and M. Jarrold, *Phys. Rev. Lett.*, 2003, **91**, 215508.
- 14 G. Breaux, D. Hillman, C. Neal, R. Benirschke and M. Jarrold, *J. Am. Chem. Soc.*, 2004, **126**, 8628–8629.
- 15 S. Chacko, K. Joshi, D. Kanhere and S. Blundell, *Phys. Rev. Lett.*, 2004, **92**, 135506.
- 16 S. Krishnamurty, S. Chacko, D. Kanhere, G. Breaux, C. Neal and M. Jarrold, *Phys. Rev. B: Condens. Matter Mater. Phys.*, 2006, **73**, 045406.

- 17 S. Krishnamurty, K. Joshi, S. Zorriasatein and D. G. Kanhere, *J. Chem. Phys.*, 2007, **127**, 054308.
- 18 S. Núñez, J. López and A. Aguado, *Nanoscale*, 2012, **4**, 6481–6492.
- 19 K. Steenbergen, D. Schebarchov and N. Gaston, *J. Chem. Phys.*, 2012, **137**, 144307.
- 20 D. Schebarchov and N. Gaston, *Phys. Chem. Chem. Phys.*, 2012, **14**, 9912–9922.
- 21 F. Baletto and R. Ferrando, *Rev. Mod. Phys.*, 2005, **77**, 371.
- 22 A. Aguado and M. Jarrold, *Annu. Rev. Phys. Chem.*, 2011, **62**, 151–172.
- 23 C. Neal, A. Starace and M. Jarrold, *Phys. Rev. B: Condens. Matter Mater. Phys.*, 2007, **76**, 54113.
- 24 U. Röthlisberger and W. Andreoni, *J. Chem. Phys.*, 1991, **94**, 8129.
- 25 B. Assadollahzadeh, S. Schäfer and P. Schwerdtfeger, *J. Comput. Chem.*, 2010, **31**, 929–937.
- 26 B. Song and P. lin Cao, *J. Chem. Phys.*, 2005, **123**, 144312.
- 27 F. Chuang, C. Wang and K. Ho, *Phys. Rev. B: Condens. Matter Mater. Phys.*, 2006, **73**, 125431.
- 28 R. Poteau, F. Spiegelmann and P. Labastie, *Z. Phys. D: At., Mol. Clusters*, 1994, **30**, 57–68.
- 29 A. Aguado, J. López, J. Alonso and M. Stott, *J. Chem. Phys.*, 1999, **111**, 6026.
- 30 F. Calvo and F. Spiegelmann, *Phys. Rev. Lett.*, 1999, **82**, 2270–2273.
- 31 F. Calvo and F. Spiegelmann, *J. Chem. Phys.*, 2000, **112**, 2888.
- 32 D. Wales and R. Berry, *J. Chem. Phys.*, 1990, **92**, 4283.
- 33 T. Beck, D. Leitner and R. Berry, *J. Chem. Phys.*, 1988, **89**, 1681.
- 34 T. Beck and R. Berry, *J. Chem. Phys.*, 1988, **88**, 3910.
- 35 F. Calvo, J. Galindez and F. Gadéa, *J. Phys. Chem. A*, 2002, **106**, 4145–4152.
- 36 I. Garzón and J. Jellinek, *Z. Phys. D: At., Mol. Clusters*, 1991, **20**, 235–238.
- 37 I. Garzón, I. Kaplan, R. Santamaria and O. Novaro, *J. Chem. Phys.*, 1998, **109**, 2176.
- 38 V. Bonačić-Koutecký, J. Jellinek, M. Wiechert and P. Fantucci, *J. Chem. Phys.*, 1997, **107**, 6321.
- 39 K. Joshi, D. Kanhere and S. Blundell, *Phys. Rev. B: Condens. Matter Mater. Phys.*, 2002, **66**, 155329.
- 40 R. Werner, *Eur. Phys. J. B*, 2005, **43**, 47–52.
- 41 A. Aguado, *J. Phys. Chem. B*, 2005, **109**, 13043–13048.
- 42 S. Zorriasatein, M. Lee and D. Kanhere, *Phys. Rev. B: Condens. Matter Mater. Phys.*, 2007, **76**, 165414.
- 43 F. Calvo, J. Neirotti, D. Freeman and J. Doll, *J. Chem. Phys.*, 2000, **112**, 10350.
- 44 G. Kresse and J. Hafner, *Phys. Rev. B: Condens. Matter Mater. Phys.*, 1993, **47**, 558.
- 45 G. Kresse and J. Hafner, *Phys. Rev. B: Condens. Matter Mater. Phys.*, 1994, **49**, 14251.
- 46 G. Kresse and J. Furthmüller, *Comput. Mater. Sci.*, 1996, **6**, 15–50.
- 47 G. Kresse and J. Furthmüller, *Phys. Rev. B: Condens. Matter Mater. Phys.*, 1996, **54**, 11169–11186.
- 48 J. Perdew, J. Chevary, S. Vosko, K. Jackson, M. Pederson, D. Singh and C. Fiolhais, *Phys. Rev. B: Condens. Matter Mater. Phys.*, 1992, **46**, 6671.
- 49 J. Perdew, J. Chevary, S. Vosko, K. Jackson, M. Pederson, D. Singh and C. Fiolhais, *Phys. Rev. B: Condens. Matter Mater. Phys.*, 1993, **48**, 4978.
- 50 P. Blöchl, *Phys. Rev. B: Condens. Matter Mater. Phys.*, 1994, **50**, 17953–17979.
- 51 G. Kresse and D. Joubert, *Phys. Rev. B: Condens. Matter Mater. Phys.*, 1999, **59**, 1758–1775.
- 52 C. Bichara, J. Gaspard and J. Mathieu, *Phys. Lett. A*, 1987, **119**, 462–468.
- 53 A. Ferrenberg and R. Swendsen, *Phys. Rev. Lett.*, 1988, **61**, 2635–2638.
- 54 F. Calvo and P. Labastie, *Chem. Phys. Lett.*, 1995, **247**, 395–400.
- 55 R. Bader, *Atoms in Molecules: a quantum theory, International series of monographs on chemistry*, Clarendon Press, Oxford, UK, 1990, vol. 22.
- 56 B. Silvi and A. Savin, *Nature*, 1994, **371**, 683–685.
- 57 A. Savin, R. Nesper, S. Wengert and T. Fässler, *Angew. Chem., Int. Ed. Engl.*, 1997, **36**, 1808–1832.
- 58 A. Savin, A. Becke, J. Flad, R. Nesper, H. Preuss and H. V. Schnerring, *Angew. Chem., Int. Ed. Engl.*, 1991, **30**, 409–412.
- 59 M. Schmidt, J. Donges, T. Hippler and H. Haberland, *Phys. Rev. Lett.*, 2003, **90**, 103401.
- 60 M. Brack, *Rev. Mod. Phys.*, 1993, **65**, 677–732.